Separation and Purification Technology 257 (2021): 117974

DOI: https://doi.org/10.1016/j.seppur.2020.117974

Carbon-encapsulated iron nanoparticles as reusable adsorbents for micropollutants removal from water

Macarena Munoz[1,], Julia Nieto-Sandoval[1], Silvia Álvarez-Torrellas[2], Eva Sanz-Santos[2], Blanca Calderón[3], Zahara M. de Pedro[1], Marcos Larriba[2], Andrés Fullana[3], Juan García[2] and Jose A. Casas[1]*

[1]Chemical Engineering Department, Universidad Autonoma de Madrid, Ctra. Colmenar km 15, 28049 Madrid, Spain

[2]Chemical Engineering Department, Universidad Complutense de Madrid, Avda. Complutense s/n, 28040 Madrid, Spain

[3]Chemical Engineering Department, University of Alicante, San Vicente del Raspeig Road, s/n 03690 San Vicente del Raspeig, Alicante, Spain

*Corresponding author phone: +34 91 497 3991; fax: +34 91497 3516; e-mail: macarena.munnoz@uam.es

Keywords: Adsorption; CWPO; carbon-encapsulated iron nanoparticles; micropollutant.

Graphical abstract

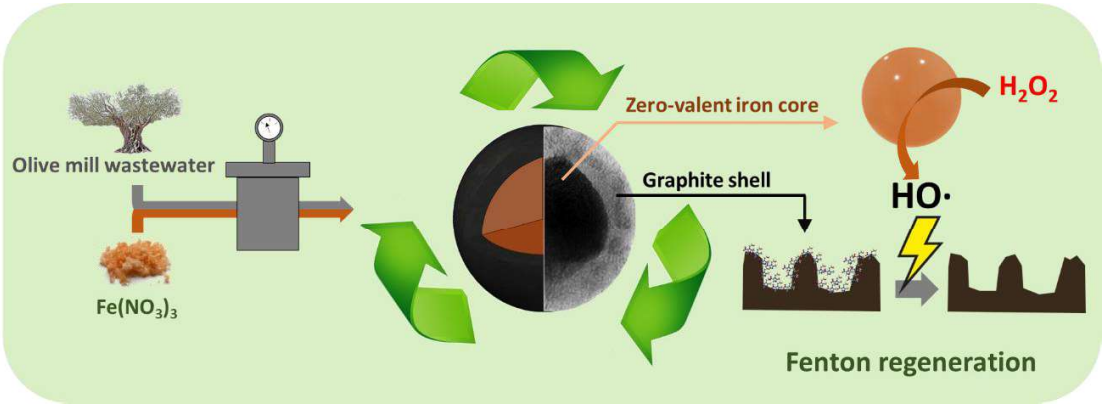

Abstract

Adsorption represents the most plausible technology for micropollutants removal from water nowadays. Nevertheless, the regeneration of the saturated carbon materials is still an important challenge, being these solids in practice commonly disposed. This work aims at overcoming this issue by using innovative carbon-encapsulated iron nanoparticles (CE-nFe). This material was synthesized by a low-cost and green method *viz.* hydrothermal carbonization (HTC), using olive mill wastewater as carbonaceous source. The solid was fully characterized by different techniques (magnetic properties, elemental analyses, N_2-sorption isotherms, pH_{PZC}, ICP, XRD and TEM). It showed a clear core-shell structure of around 40 nm in diameter. The core was mainly formed by zero-valent iron and the shell by graphitized carbon. Accordingly, it showed an essentially mesoporous structure, with a specific surface area of 169 $m^2\ g^{-1}$, and a clear hydrophobic character (pH_{PZC} = 10). Its adsorption performance was investigated using three relevant micropollutants (diclofenac (DCF), sulfamethoxazole (SMX) and metronidazole (MNZ)). A very fast removal of the micropollutants was achieved (30 min at the most, with rate constants in the range of $0.11 - 0.41$ g $mg^{-1}\ min^{-1}$). The adsorption isotherms revealed the vertical packing of the adsorbate molecules onto the adsorbent active centers, being the data successfully described by the GAB model. The saturated adsorbents were effectively regenerated by heterogeneous Fenton oxidation, taking advantage of the iron core of CE-nFe and the opened mesoporous carbon shell. The regeneration efficiency increased with increasing the operating temperature ($25 - 75$ ºC) and contact time ($1 - 4$ h), as well as the H_2O_2 dose up to 6 g L^{-1}. The micropollutant nature affected the adsorbent regeneration yield in the order: SMX>DCF>MNZ, consistent with their reactivity towards Fenton oxidation.

1. Introduction

The widespread occurrence of micropollutants in aquatic ecosystems has become an issue of major concern for both the environment and public health. Micropollutants family encompasses a vast array of substances, mainly anthropogenic, such as pharmaceuticals, hormones, personal care products, flame retardants or pesticides, among other [1, 2]. These compounds, habitually present in urban wastewaters, cannot be completely removed in current wastewater treatment plants (WWTPs) due their high persistence and non-biodegradability character [1, 3, 4]. Once in the aquatic environment, even at the frequently low concentrations encountered (ng/L or μg/L), they can impact the organisms and ecosystem balance given their high bioactivities, and also affect drinking water resources [3, 5-9].

The development of advanced processes that warrant the complete removal of these pollutants at the sources, mainly WWTPs, represents an important challenge nowadays. Many alternatives have been so far explored, being Advanced Oxidation Processes (AOPs), and in particular ozonation, photocatalysis and Fenton-based technologies, the main field of research [2, 3, 10-13]. Nevertheless, adsorption is still considered the most plausible process for micropollutants removal, probably due to the expensive reagents/energy requirements of AOPs, the possible generation of harmful by-products and the lack of full-scale applications. In fact, in Switzerland, where micropollutants elimination (at least, 80%) is mandatory since 2016, WWTPs have been mainly optimized by including adsorption tertiary treatments, being so far scarce the implementation of AOP units [14].

Activated carbons (ACs) are clearly the most extendedly used adsorbents for water treatment, which can be explained by their outstanding properties *i.e.* large specific surface areas (500 – 1500 $m^2\ g^{-1}$), high pore volumes (>0.5 $cm^3\ g^{-1}$) and relatively low-cost (~1500 € ton^{-1}) given their commonly natural origin [15-21]. The essentially microporous structure of these materials leads to extremely high adsorption

capacity values (several hundreds of mg per g_{AC}), but unavoidably involves slow pollutant uptakes (of the order of hours) due to diffusion limitations [20, 22, 23]. Another important issue dealing with the application of these materials is the management of the saturated adsorbents. Direct disposal is a common practice as the effective regeneration of the solids represents a significant challenge. Thermal regeneration processes, which are usually performed at high temperatures (500 – 900 ºC), require considerable energy consumption and are usually accompanied by important carbon losses [24, 25]. Desorption procedures, based on the variation of pressure, solvent polarity and pH could overcome those drawbacks [13, 26]. Among them, solvent regeneration, typically with acetone and methanol, has proved to be quite effective [27, 28]. Nevertheless, all these regeneration methods lead to a concentrated solution of the pollutants, which requires further management/treatment. In this context, the application of a direct destructive technique at softer conditions than the thermal treatments, is desirable from both economic and environmental sides.

Degradation-based AOP technologies, in particular Fenton oxidation, appear as a potential solution for adsorbent regeneration. Although bare carbon materials can act as Fenton catalysts [29], their activity is orders of magnitude lower than the achieved with active metal species, mainly Fe oxides [30, 31]. Consequently, regeneration of spent ACs has been mainly explored by the addition of Fenton's reagent ($Fe^{3+/2+}/H_2O_2$). Nevertheless, the obtained efficiencies are usually below ~60% [32-35] due to the microporous structure of ACs, which leads to relevant diffusion limitations. Xiao et al. [21] recently demonstrated that the pore structure of carbon materials plays a key role on their regeneration, being the mesoporous solids the most appropriate for such goal (efficiency above 90%). Instead of applying Fe amendments, these authors directly used carbon supports decorated with γ-Fe_2O_3 particles. The adsorption efficiency was evaluated using methyl orange dye as target pollutant.

The aim of this study is the application of innovative mesoporous carbon-encapsulated magnetic iron nanoparticles (CE-nFe) as reusable adsorbents for the removal of micropollutants from water. This material was synthesized by a low-cost and green method *viz.* hydrothermal carbonization (HTC), using

olive mill wastewater as carbonaceous source [36]. Three representative pharmaceuticals (diclofenac (DCF), metronidazole (MNZ) and sulfamethoxazole (SMX)) were selected as target pollutants in order to evaluate the effect of their nature on the adsorbent regeneration by heterogeneous Fenton oxidation. The adsorption capacity and kinetics of CE-nFe were firstly analyzed. Subsequently, the efficiency of heterogeneous Fenton regeneration under different operating conditions (H_2O_2 concentration, temperature and contact time) was investigated in regeneration-adsorption cycles.

2. Materials and methods

2.1. Synthesis and characterization of carbon-encapsulated iron nanoparticles

The synthesis procedure of CE-nFe was based on a previous work [36], in which iron(III) nitrate was reduced by hydrothermal reaction with olive mill wastewater. This carbon source was obtained from an olive mill company of Extremadura region (Spain). Prior use, it was centrifuged at 5000 rpm for 30 min, and then filtrated with a 8 μm fiber glass filter. Briefly, 300 mL olive mill wastewater and 0.057 mol $Fe(NO_3)_3 \cdot 9H_2O$ were mixed for 1 h by mechanical stirring. The resulting solution was then transferred to a 1 L HTC reactor (FCF-1, Zhengzhou Keda Machinery), which was heated up to 225 ºC and kept for 3 h. Afterwards, the reactor was cooled down and the obtained mixture was vacuum filtered (0.2 μm cellulose acetate filter) and washed twice with a 50/50 (v/v) ethanol-water solution. The solid fraction was then dried at 80 ºC for 12 h and grounded into fine powder. In order to develop mesoporosity on the carbon shell and increase the zero-valent iron content of the particles, the solid was finally activated in a rotatory reactor at 800ºC under anaerobic conditions. Specifically, the particles were inserted into a quartz tube and treated during 3 h at the selected temperature under a nitrogen mass flow of 500 mL min^{-1}.

The porous structure of CE-nFe was characterized from N_2 sorption isotherms at -196 ºC employing a Micromeritics Tristar 3020 apparatus. Prior analysis, the samples were outgassed overnight at 150 ºC under vacuum (10^{-5} – 10^{-6} Torr). The crystalline phase of the CE-nFe iron core was analyzed by X-ray diffraction (XRD) using a Siemens diffractometer (model D-5000) with Cu Kα radiation in the 2θ range

from 10 to 80°. The total iron content of the material was determined by inductively coupled plasma (ICP/MS, ICP-MS Elan 6000 PerkinElmer Sciex). Elemental analysis was performed in an Elemental Analyzer LECO CHNS-932. The magnetic properties of CE-nFe were determined by a superconducting quantum interference device (SQUID) (Quantum Design MPMS XL-5). Transmission electron microscopy (TEM) images were obtained using a JEOL JEM-2010 microscope. The particle size distribution was measured by laser granulometry using a Mastersizer 3000 (MALVERN). The point of zero charge of the solid was calculated following a procedure described elsewhere [37].

2.2. Adsorption tests

Adsorption experiments were carried out at 25 ºC in 100 mL glass bottles shaken in a thermostatic bath (Julabo SW22) at 200 rpm. Both kinetic and equilibrium adsorption tests were performed to determine the equilibrium time and adsorption isotherms of the micropollutants onto CE-nFe. In both cases, an initial micropollutant concentration of 100 mg L^{-1} and a volume of 50 mL were used. The dose of adsorbent was fixed at 0.6 mg mL^{-1} in the kinetic runs while it was varied from 0.05 to 4 mg mL^{-1} in the equilibrium adsorption tests. All experiments were carried out by triplicate, being the standard deviation less than 10% in all cases.

To confirm that the carbon-shell of CE-nFe was the responsible for micropollutants adsorption, a preliminary experiment with bare iron nanoparticles was carried out under the same operating conditions previously mentioned using DCF as target pollutant. The adsorption capacity of bare iron nanoparticles was below 1 mg g^{-1}. Therefore, the adsorption performance of CE-nFe can be directly related with the properties of its carbon shell.

The equilibrium adsorption capacity (mg g^{-1}) of CE-nFe with each of the micropollutants tested was calculated by the following Eq. (1):

$$q_e = \frac{(C_0 - C_e)}{W} \cdot V \qquad (1)$$

where q_e (mg g^{-1}) is the equilibrium adsorption capacity; C_0 (mg L^{-1}) is the initial micropollutant concentration; C_e (mg L^{-1}) is the equilibrium micropollutant concentration; V (L) is the solution volume and W (g) is the adsorbent weight.

2.3. Adsorbent regeneration procedure

Adsorbent regeneration runs were carried out with pre-saturated solids. To saturate the adsorbent, the fresh solid (300 mg) was suspended in a 500 mL micropollutant solution (100 mg L^{-1}) for 24 h at 25 ºC in a thermostatic bath (200 rpm). Afterwards, the solution was filtrated and the solid was dried at 60 ºC overnight. Regeneration tests were then performed at varying temperatures (25, 50 and 75 ºC), H_2O_2 concentrations (3, 6 and 9 g L^{-1}) and contact times (1, 4, 20 h) with the aim of evaluating their influence on the kinetics and adsorption capacity recovery of the materials. A 500 mL solution with the saturated adsorbent at a concentration of 0.25 g L^{-1} was used in all cases. These runs were also accomplished in thermostatic bath (200 rpm), at pH_0=3.

2.4. Analytical methods

The evolution of the adsorption experiments was carried out by periodically taking and analyzing liquid samples from the reactor. The adsorbent was previously separated by filtration (PTFE 0,45 μ Syringe Filter). Micropollutants concentration was determined by high performance liquid chromatography (Shimadzu, mod. Prominence-i, LC-2030C LT) with diode array detector (SPDM30A). An Eclipse Plus C18 column (Agilent) was employed as stationary phase and the mobile phases were varied depending on the micropollutant analyzed. Mixtures of 10/90%, 25/75% and 57/43% (v/v) of acetonitrile and acetic acid aqueous solution (75 mM) were used for MNZ, SMX and DCF, respectively. All analyses were performed at 270 nm.

2.5. Evaluation of the kinetic and isotherm parameters

The experimental adsorption isotherms were fitted to several models, e.g., Langmuir, Freundlich, Sips, and Guggenheim-Anderson-de Boer (GAB). These models are described in the Supplementary Material.

The predicted adsorption capacity values by the models (q_{cal}) were compared to those obtained experimentally (q_{exp}) using the standard deviation (SD) parameter (Eq. 2) for non-linear adsorption isotherm equations, calculated by using the Solver Microsoft Excel v. 2013 software.

$$SD = \sqrt{\frac{\Sigma\left[\left(q_{\exp} - q_{cal}\right)/q_{\exp}\right]^2}{N-1}} \quad (2)$$

where N is the number of experimental points.

3. Results and discussion

3.1. Characterization of carbon-encapsulated iron nanoparticles

Fig. 1 shows the TEM images and size distribution of CE-nFe particles, whose average diameter was 40 ± 6 nm, as determined by measuring individual nanoparticles diameter in TEM images. The iron core and the thin carbon shell can be clearly distinguished in the TEM image of a single nanoparticle (Fig. 1b). Nevertheless, it must be noted that particles appeared partially aggregated, as revealed by the laser-diffraction particle-size analyser (see Fig. S1 of the Supplementary Material for experimental data). The value of D_{50} was 16.6 μm, which means that 50% of aggregates was smaller than this size. The total iron content of the material (44% wt.) was measured by ICP. This analysis also revealed the presence of Ca (4.3% wt.) and K (0.9% wt.) in the solid, which can be explained by the composition of the olive mill wastewater used in the synthesis [36]. Consistent with this result, the elemental composition of the material corresponded to C (35% wt.), H (0.4% wt.), N (0.6% wt.) and S (0.2% wt.). An oxygen content of 14.6% wt. was calculated by difference.

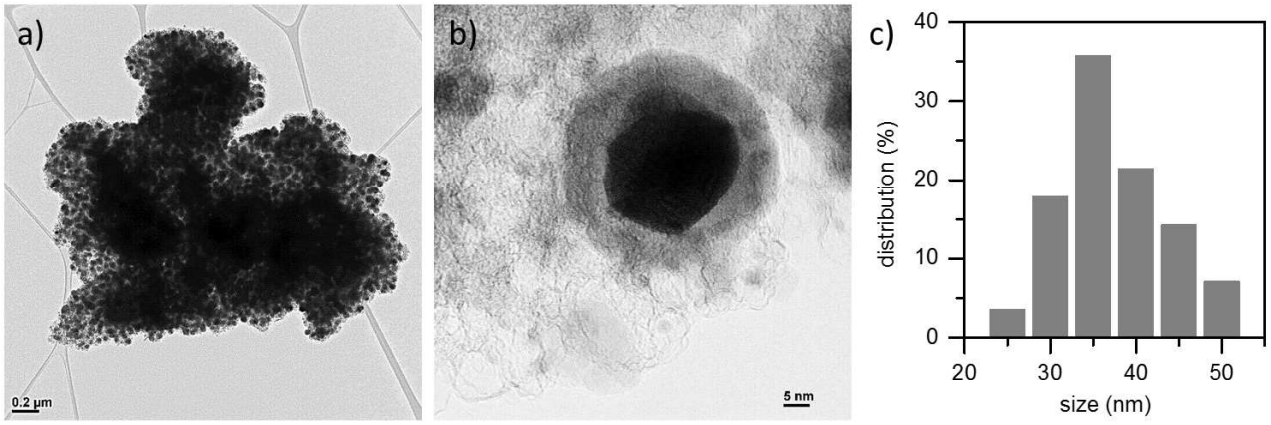

Fig. 1. TEM images of CE-nFe particles (a, b) and CE-nFe particle size distribution (c).

The specific surface area of the material was 169 m^2 g^{-1}. It showed a clear mesoporous character, giving rise to a type IV N_2 sorption isotherm according to IUPAC classification (Fig. 2a). Accordingly, the mesoporores volume was 0.19 cm^3 g^{-1} while that of micropores was around ten-fold lower (0.02 cm^3 g^{-1}). The iron core of the nanoparticles provided strong magnetic properties to the resulting CE-nFe material, whose magnetization hysteresis loop is shown in Fig. 2b. The calculated magnetization saturation (M_S), coercivity (H_C) and saturation remanence (M_R) values were 33 emu g^{-1}, 184.5 Oe and 2.2 emu g^{-1}, respectively. These magnetic properties are of interest since they warrant the complete separation and recovery of the adsorbent from the water phase by the application of a magnetic field. On the other hand, according to the XRD pattern of the material, zero-valent iron, graphite and austenite were the main crystalline phases present in the solid (Fig. 2c). They were identified using ICDD PDFs 00-006-0696, 00-001-0646 and 00-023-0298, respectively. The occurrence of zero-valent iron in the solid is consistent with the raw materials and the synthesis procedure followed [36]. The appearance of graphite and austenite can be related to the post-treatment of the solid at high temperature (800 ºC), used in this work with the aim of developing mesoporosity in the carbon shell and at the same time increase the zero-valent iron proportion in the particles. The presence of graphite confirms the high structural order in the carbon shell of CE-nFe, typical of mesoporous carbon materials. Other peaks present in the XRD pattern were related to other minor crystalline phases like calcite and calcium phosphate, which is consistent with the

abovementioned Ca content of the solid. In the same line, cohenite and iron phosphide were also observed.

To complete the adsorbent characterization, the pH_{PZC} value was also measured. A clearly basic/hydrophobic character (pH_{PZC} = 10) was found. This feature represents an additional advantage for CE-nFe application in water treatment, as it would avoid unfavorable interactions with water molecules, which is essential for the efficient organic micropollutants adsorption [3].

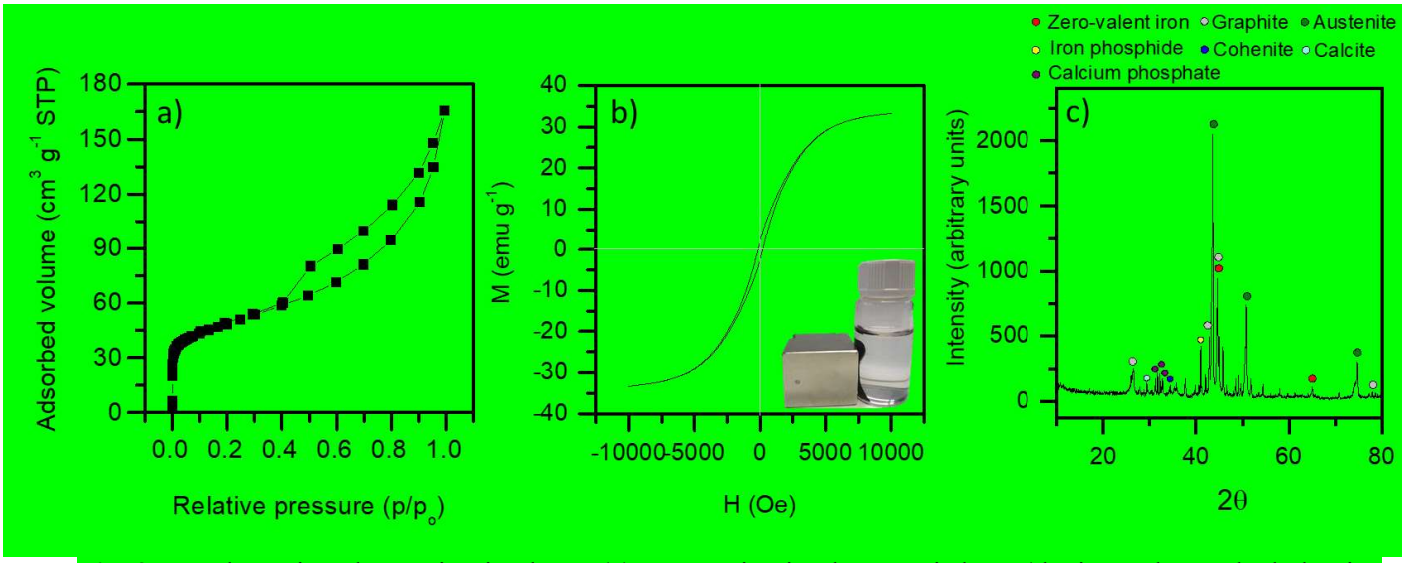

Fig. 2. N_2 adsorption-desorption isotherm (a), magnetization hysteresis loop (the inset shows the behavior of the sample under a magnetic field) (b) and X-ray diffraction pattern (c) of CE-nFe.

3.2. Adsorption performance: Capacity and kinetics

The adsorption isotherms of SMX, DCF and MNZ onto the CE-nFe material are depicted in Fig. 3. In all cases, the initial micropollutant concentration was established at 100 mg L^{-1} while the adsorbent dose was varied in the range of 0.05 – 4 mg mL^{-1}. A clear sigmoidal shape was observed in all isotherms, which can be categorized as subtype S-3 according to Giles classification [38]. This fact is indicative of a weak interaction between micropollutants and CE-nFe surface at low solute concentrations and multilayer adsorption behavior at high solute concentrations. The occurrence of this phenomenon is reasonable given the essentially mesoporous character of the material, which allows the formation of several adsorbate layers onto its surface. The adsorption capacity values achieved by the CE-nFe material were not as remarkable as those exhibited by conventional microporous activated carbons [22, 23, 39, 40], which can

be related to its significantly lower specific surface area (169 *vs.* 500-1000 m^2 g^{-1}). Nevertheless, these values are comparable to the reported for other mesoporous activated carbons of similar specific surface areas [41, 42]. For instance, Hu et al. [41] obtained a maximum DCF adsorption capacity of 24 mg g^{-1} using multi-walled carbon nanotubes (190 m^2 g^{-1}).

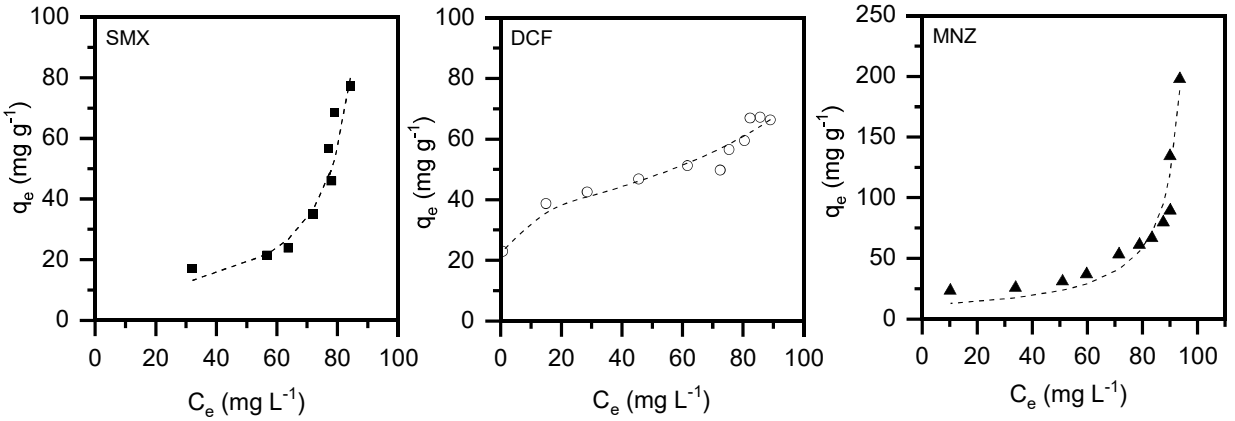

Fig. 3. Experimental (symbols) and fitted (solid lines) data for the equilibrium adsorption isotherms of SMX, DCF and MNZ onto CE-nFe nanoparticles ([micropollutant]$_0$ = 100 mg L^{-1}; [CE-nFe] = 0.05 – 4 mg mL^{-1}).

Different empirical adsorption models such as Freundlich, Langmuir, Sips and Guggenheim-Anderson de Boer (GAB) were used to fit the experimental data. The adsorption parameters obtained with all the models tested can be seen in the Supplementary Material (Table S1). The GAB model clearly showed the most accurate description of the isotherms data. The results obtained are depicted in Fig. 3. This model is commonly used for the fitting of multilayer isotherms while Langmuir and Freundlich models assume the adsorption as the formation of a monolayer adsorbate onto the adsorbent surface [38]. In this work, a plateau was observed up to a threshold value of 60 – 80 mg L^{-1} micropollutant concentration, indicating the monolayer completion. At higher micropollutant concentrations, a clear sigmoidal trend was found, which can be related to the multilayer adsorption and vertical packing of the adsorbate molecules onto the adsorbent centers. This behavior is typical of mesoporous materials [43]. The effect was clearly more evident with MNZ and SMX compared to DCF. This could be explained by

the different molecular size of the micropollutants, which followed the order: DCF (0.354 nm^3) > SMX (0.278 nm^3) > MNZ (0.215 nm^3). Taking into account that the mean pore size of CE-nFe nanoparticles was around 3 nm, it is clear that the addition of a higher number of molecule layers inside the pores was then more favored with smaller molecules (SMX and MNZ).

Once evaluated the adsorption capacity of CE-nFe with the three micropollutants, a kinetic study was performed. Clearly, the mesoporous character of this material represented an important advantage compared to conventional activated carbons in terms of adsorption rate. As can be seen in Fig. 4, CE-nFe allowed to reach considerably fast adsorption micropollutant uptakes from water. More than 90% of the equilibrium uptake was achieved with the three compounds tested in only 5 min, while several hours are commonly required when microporous activated carbons are used [22, 39]. The experimental data were properly described by the pseudo-second order kinetic rate equation. The obtained rate constants for SMX, MNZ and DCF removal were 0.41, 0.32 and 0.11 g mg^{-1} min^{-1}, respectively. The differences among them seem to be associated to the size of the molecules (MNZ<SMX<DCF) as well as to their hydrophobic character (pKa_{MNZ}=2.4; pKa_{DCF}=4.0; pKa_{SMX}=5.7). All in all, these rate constant values are significantly higher than the reported in the literature with conventional activated carbons. Ahmed et al. [23] obtained rate constant values in the range of 1 x 10^{-3} – 3.9 x 10^{-3} g mg^{-1} min^{-1} in the removal of MNZ (20 – 100 mg L^{-1}) by a microporous seed-based AC. In the same line, Bhadra et al. [22] reported rate constant values of 0.2 x 10^{-3} g mg^{-1} min^{-1} for the adsorption of DCF (100 mg L^{-1}) onto oxidized AC. Similarly, Çaliskan et al. [40] achieved rate constant values within the range of 1.27 x 10^{-4} – 7.11 x 10^{-5} g mg^{-1} min^{-1} in SMX (10 – 20 mg L^{-1}) adsorption using a commercial coal-based AC. The mesoporous structure of CE-nFe as well as its strong hydrophobic character seem to be the reasons for the high adsorption rates achieved compared to conventional activated carbons. In fact, the results obtained in the current work are consistent with those achieved in a prior contribution, where the effect of the carbon structure on its adsorption performance was evaluated by using well-defined carbide-derived carbons (CDCs) [39]. It was

demonstrated that while the specific surface area played a key role on the adsorption capacity of the adsorbent, the pore size determined the rate of the process. In this sense, the essentially mesoporous CDC led to a DCF adsorption rate constant value up to 15 times higher than the microporous one (7.7×10^{-3} *vs.* 0.5×10^{-3} g mg^{-1} min^{-1}).

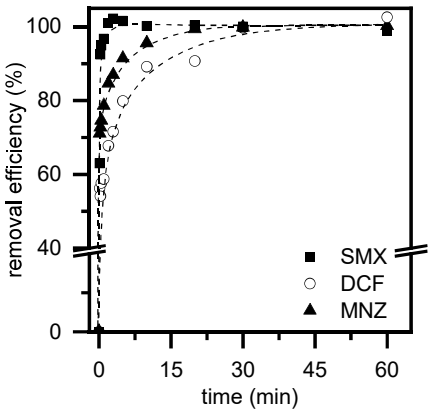

Fig. 4. Rate of micropollutants uptake onto CE-nFe nanoparticles in deionized water ($[micropollutant]_0$ = 100 mg L^{-1}; [CE-nFe] = 0.6 mg mL^{-1}).

3.3. Heterogeneous Fenton regeneration

Prior to the evaluation of the adsorbent regeneration by Fenton oxidation, direct application of the used adsorbents (without any kind of regeneration) was carried out. A significant loss of their adsorption capacity was found in all cases, which is consistent with the reduction of the available adsorption sites at the surface of the material. As representative example, the adsorption capacity of the solid decreased from 66 to 11 mg g^{-1} when DCF was used as target pollutant. Clearly, regeneration of the adsorbent is required to allow its reusability.

The adsorbent regeneration by heterogeneous Fenton oxidation was evaluated taking advantage of the ability of the iron core of CE-nFe to decompose H_2O_2 leading to the generation of hydroxyl radicals. The effect of H_2O_2 concentration (3000 – 9000 mg L^{-1}), operating temperature (25 – 75 ºC) and contact time (1 – 4 h) on adsorbent regeneration were analyzed. All these factors were separately investigated at the following standard conditions: 3000 mg L^{-1} H_2O_2, 25 ºC and 1 h. After each of the regeneration

experiments, the adsorption behavior of the regenerated adsorbents was tested using the same conditions previously described for the kinetic experiments ([micropollutant]$_0$ = 100 mg L^{-1}; [CE-nFe] = 0.6 mg mL^{-1}). The main results obtained are summarized in Fig. 5.

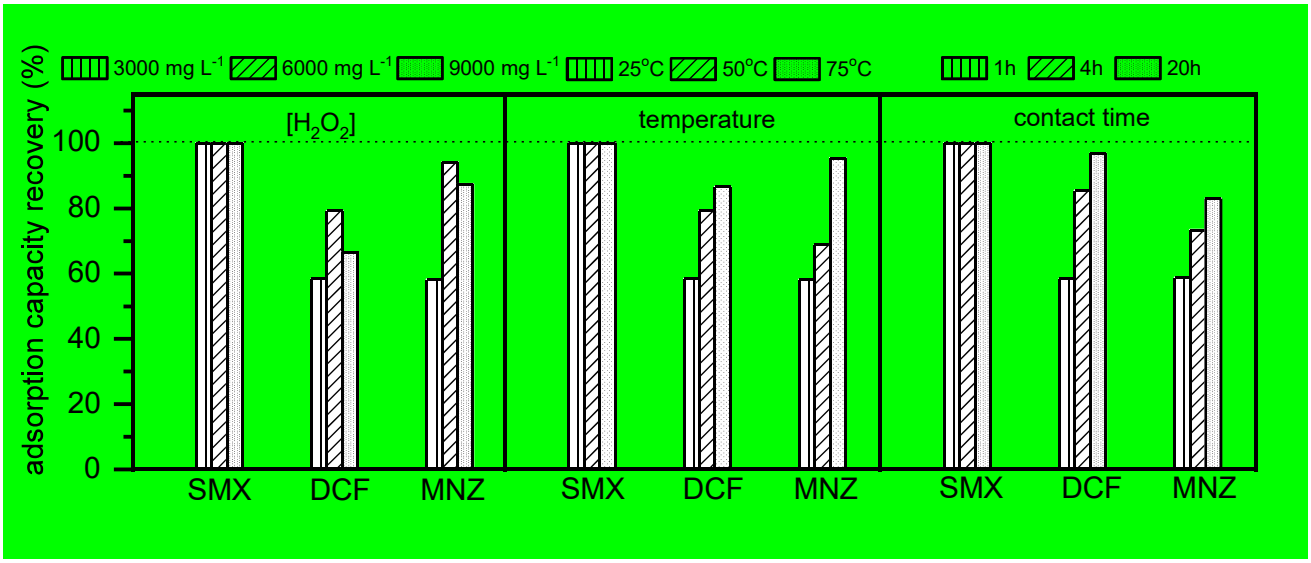

Fig. 5. Impact of regeneration conditions on the recovery of the CE-nFe adsorption capacity for the removal of SMX, MNZ and DCF (adsorption conditions: [micropollutant]$_0$ = 100 mg L^{-1}; [CE-nFe] = 0.6 mg mL^{-1}; standard regeneration conditions: [H_2O_2]$_0$ = 3000 mg L^{-1}; T = 25 ºC; t = 1 h).

The operating conditions used in the regeneration experiments showed an important effect on the adsorption capacity recovery of the solid. As complete regeneration of the adsorbent was achieved with SMX regardless of the conditions used, the discussion will be focused on the results obtained with DCF and MNZ. In both cases, In both cases, the increase of temperature and/or contact time during the regeneration experiments allowed to recover the original adsorption capacity of the solid to a major extent, which can be explained by the higher removal yield of the adsorbates from the surface. Nevertheless, in the case of H_2O_2, a clear increase in the recovery of the adsorption capacity was achieved by increasing the H_2O_2 concentration from 3 to 6 g L^{-1} while a higher concentration (9 g L^{-1}) led to a decrease on the adsorption capacity of regenerated CE-nFe. The characterization of these regenerated adsorbents revealed that the main reason behind this finding seems to be the generation of oxygen groups at their surface. The

pH_{PZC} of the regenerated adsorbents decreased with increasing the H_2O_2 concentration employed in the regeneration experiments. For instance, in the regeneration of the adsorbent saturated with DCF, the pH_{PZC} decreased from a value of 10 of the fresh catalyst to 8.2, 7.0 and 5.7 with H_2O_2 concentrations of 4, 6 and 9 g L^{-1}, respectively. The presence of carboxylic groups at the adsorbent surface lead to competitive effects with water molecules, avoiding the efficient adsorption of the organic pollutants. It must be noted that other properties of the adsorbents remained almost unchanged after the regeneration process. The loss of iron was practically negligible (<0.1% of the initial iron content) and the thermogravimetric analyses did not show any loss of carbon percentage.

To further evaluate the reusability of the adsorbent, consecutive adsorption-regeneration experiments were carried out using SMX as target pollutant. The regeneration procedure was performed at two different temperatures (25 and 75 ºC) using a H_2O_2 concentration of 3000 mg L^{-1} and a contact time of 1 h. Remarkably, the adsorption capacity of the adsorbent remained almost unchanged (>99%) when the adsorbent was regenerated at 75 ºC. Nevertheless, when the regeneration was carried out at ambient conditions, the adsorption capacity was reduced from 100% in the first run to 86% and 63% in the second and third runs, respectively. These results allow to confirm that the adsorbent can be reused in consecutive regeneration-adsorption cycles although intensified conditions are required to completely restore the initial adsorption capacity of the solid. It must be noted that iron leaching along these consecutive experiments was practically negligible. On the other hand, the thermogravimetric analyses of the used adsorbents did not reveal the appearance of new species, possibly due to the low concentration of micropollutants present at the adsorption sites of the adsorbent regenerated at ambient conditions.

On the other hand, the appearance of new peaks was not observed in the thermogravimetric analyses.

The significant differences found on the adsorbent regeneration yield with the three micropollutants tested can be related to their reactivity towards the hydroxyl radicals generated in the Fenton oxidation treatment. The clear trend observed (SMX>DCF>MNZ) is consistent with the previously reported in the

literature in heterogeneous Fenton oxidation process [44, 45]. In any case, under the optimized regeneration conditions (75 ºC, 6000 mg L^{-1} H_2O_2 and 20 h contact time), at least 95% regeneration of the solid was achieved for all the micropollutants/adsorbent tested. It must be also highlighted that the rate of the process was not varied after the regeneration process. As representative example, the results obtained in the adsorption of SMX with the fresh and regenerated adsorbent (at regenerating conditions: 25ºC, 1h contact time and 3000 mg L^{-1} H_2O_2) can be seen in Fig. 6. Clearly, the adsorption rate remained almost unchanged when the regenerated adsorbent was used, obtaining a pseudo-second order constant value of 0.36 g mg^{-1} min^{-1}.

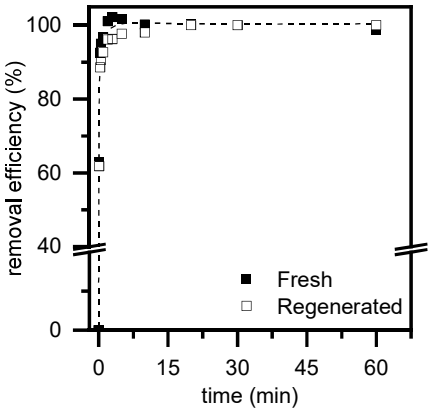

Fig. 6. Impact of regeneration conditions on the kinetics of CE-nFe for the removal of SMX ($[micropollutant]_0$ = 100 mg L^{-1}; [CE-nFe] = 0.6 mg mL^{-1}).

4. Conclusions

The inexpensive CE-nFe material, composed by a zero-valent iron core and a graphitized carbon shell, has proved to be an effective and reusable adsorbent for organic micropollutants removal. Its outstanding properties *viz.* mesoporous structure, hydrophobic character and magnetic properties, allowed an extremely fast removal of the micropollutants and also warranted the simple separation of the particles from water by the application of a magnetic field. Although the moderately low specific surface area of the adsorbent (169 m^2 g^{-1}) led a to a relatively low adsorption capacity, its mesoporous structure allowed

its effective regeneration by heterogeneous Fenton oxidation taking advantage of the iron core of the solid. The adsorption performance of the solid in terms of capacity and kinetics, was completely restored although significant differences were found depending on the micropollutant nature. The observed trend (SMX>DCF>MNZ) was consistent with the reactivity of such compounds towards Fenton oxidation. All in all, up to 95% regeneration was achieved in all trials by varying the regeneration conditions. The H_2O_2 concentration was the most important variable to be considered in the regeneration process as an excessive concentration led to a significant oxidation of the carbon surface, reducing the pH_{PZC} of the solid and thus, the recovery of its adsorption capacity.

Acknowledgments

This research has been supported by the Spanish MINECO through the project CTM-2016-76454-R and by the CM through the project P2018/EMT-4341. M. Munoz and J. Nieto-Sandoval thank the Spanish MINECO for the Ramón y Cajal postdoctoral contract (RYC-2016-20648) and the FPI predoctoral grant (BES-2017-081346), respectively.

Conflicts of interest

There are no conflicts to declare.

References

[1] T. Deblonde, C. Cossu-Leguille, P. Hartemann, Emerging pollutants in wastewater: A review of the literature, Int. J. Hyg. Environ. Health 214 (2011) 442-448.

[2] O.M. Rodriguez-Narvaez, J.M. Peralta-Hernandez, A. Goonetilleke, E.R. Bandala, Treatment technologies for emerging contaminants in water: A review, Chem. Eng. J. 323 (2017) 361-380.

[3] Y. Luo, W. Guo, H.H. Ngo, L.D. Nghiem, F.I. Hai, J. Zhang, S. Liang, X.C. Wang, A review on the occurrence of micropollutants in the aquatic environment and their fate and removal during wastewater treatment, Sci. Total Environ. 473-474 (2014) 619-641.

[4] P. Verlicchi, M. Al Aukidy, E. Zambello, Occurrence of pharmaceutical compounds in urban wastewater: Removal, mass load and environmental risk after a secondary treatment—A review, Sci. Total Environ. 429 (2012) 123-155.

[5] R.P. Schwarzenbach, B.I. Escher, K. Fenner, T.B. Hofstetter, C.A. Johnson, U. von Gunten, B. Wehrli, The Challenge of Micropollutants in Aquatic Systems, Science 313 (2006) 1072.

[6] A. Gogoi, P. Mazumder, V.K. Tyagi, G.G. Tushara Chaminda, A.K. An, M. Kumar, Occurrence and fate of emerging contaminants in water environment: A review, Groundwater Sustainable Dev. 6 (2018) 169-180.

[7] D.J. Lapworth, N. Baran, M.E. Stuart, R.S. Ward, Emerging organic contaminants in groundwater: A review of sources, fate and occurrence, Environ. Pollut. 163 (2012) 287-303.

[8] B.I. Escher, R. Baumgartner, M. Koller, K. Treyer, J. Lienert, C.S. McArdell, Environmental toxicology and risk assessment of pharmaceuticals from hospital wastewater, Water Res. 45 (2011) 75-92.

[9] Ismael Rodea-Palomares, Miguel Gonzalez-Pleiter, Soledad Gonzalo, Roberto Rosal, Francisco Leganes, Sergi Sabater, Maria Casellas, Rafael Muñoz-Carpena, Francisca Fernández-Piñas, Hidden drivers of low-dose pharmaceutical pollutant mixtures revealed by the novel GSA-QHTS screening method, Sci. Adv. 2 (2016) e1601272.

[10] C. Gadipelly, A. Pérez-González, G.D. Yadav, I. Ortiz, R. Ibáñez, V.K. Rathod, K.V. Marathe, Pharmaceutical industry wastewater: Review of the technologies for water treatment and reuse, Ind. Eng. Chem. Res.,53 (2014) 11571-11592.

[11] A. Mirzaei, Z. Chen, F. Haghighat, L. Yerushalmi, Removal of pharmaceuticals from water by homo/heterogonous Fenton-type processes – A review, Chemosphere 174 (2017) 665-688.

[12] M.O. Barbosa, N.F.F. Moreira, A.R. Ribeiro, M.F.R. Pereira, A.M.T. Silva, Occurrence and removal of organic micropollutants: An overview of the watch list of EU Decision 2015/495, Water Res. 94 (2016) 257-279.

[13] O. Zanella, I.C. Tessaro, L.A. Féris, Desorption- and Decomposition-Based Techniques for the Regeneration of Activated Carbon, Chem. Eng. Technol. 37 (2014) 1447-1459.

[14] J. Löwenberg, A. Zenker, T. Krahnstöver, M. Boehler, M. Baggenstos, G. Koch, T. Wintgens, Upgrade of deep bed filtration with activated carbon dosage for compact micropollutant removal from wastewater in technical scale, Water Res. 94 (2016) 246-256.

[15] A. Katsigiannis, C. Noutsopoulos, J. Mantziaras, M. Gioldasi, Removal of emerging pollutants through Granular Activated Carbon, Chem. Eng. J. 280 (2015) 49-57.

[16] J.M. Dias, M.C.M. Alvim-Ferraz, M.F. Almeida, J. Rivera-Utrilla, M. Sánchez-Polo, Waste materials for activated carbon preparation and its use in aqueous-phase treatment: A review, J. Environ. Manage. 85 (2007) 833-846.

[17] L. Zhong, Y. Zhang, Y. Ji, P. Norris, W. Pan, Synthesis of activated carbon from coal pitch for mercury removal in coal-fired power plants, J. Therm. Anal. Calorim. 123 (2016) 851-860.

[18] O. Ioannidou, A. Zabaniotou, Agricultural residues as precursors for activated carbon production—A review, Renewable Sustainable Energy Rev. 11 (2007) 1966-2005.

[19] P. Hadi, M. Xu, C. Ning, C. Sze Ki Lin, G. McKay, A critical review on preparation, characterization and utilization of sludge-derived activated carbons for wastewater treatment, Chem. Eng. J. 260 (2015) 895-906.

[20] S. Álvarez-Torrellas, M. Muñoz, J.A. Zazo, J.A. Casas, J. García, Synthesis of high surface area carbon adsorbents prepared from pine sawdust-Onopordum acanthium L. for nonsteroidal anti-inflammatory drugs adsorption, J. Environ. Manage. 183 (2016) 294-305.

[21] Y. Xiao, J.M. Hill, Impact of pore size on Fenton oxidation of methyl orange adsorbed on magnetic carbon materials: Trade-Off between capacity and regenerability, Environ. Sci. Technol. 51 (2017) 4567-4575.

[22] B.N. Bhadra, P.W. Seo, S.H. Jhung, Adsorption of diclofenac sodium from water using oxidized activated carbon, Chem. Eng. J. 301 (2016) 27-34.

[23] M.J. Ahmed, S.K. Theydan, Microwave assisted preparation of microporous activated carbon from Siris seed pods for adsorption of metronidazole antibiotic, Chem. Eng. J. 214 (2013) 310-318.

[24] F. Salvador, N. Martin-Sanchez, R. Sanchez-Hernandez, M.J. Sanchez-Montero, C. Izquierdo, Regeneration of carbonaceous adsorbents. Part I: Thermal Regeneration, Microporous Mesoporous Mater. 202 (2015) 259-276.

[25] A.L. Cazetta, O.P. Junior, A.M.M. Vargas, A.P. da Silva, X. Zou, T. Asefa, V.C. Almeida, Thermal regeneration study of high surface area activated carbon obtained from coconut shell: Characterization and application of response surface methodology, J. Anal. Appl. Pyrolysis 101 (2013) 53-60.

[26] F. Salvador, N. Martin-Sanchez, R. Sanchez-Hernandez, M.J. Sanchez-Montero, C. Izquierdo, Regeneration of carbonaceous adsorbents. Part II: Chemical, microbiological and vacuum regeneration, Microporous Mesoporous Mater. 202 (2015) 277-296.

[27] D.O. Cooney, A. Nagerl, A.L. Hines, Solvent regeneration of activated carbon, Water Res.17 (1983) 403-410.

[28] A.B. Hernández-Abreu, S. Álvarez-Torrellas, V.I. Águeda, M. Larriba, J.A. Delgado, P.A. Calvo, J. García, New insights from modelling and estimation of mass transfer parameters in fixed-bed adsorption of Bisphenol A onto carbon materials, J. Contam. Hydrol. 228 (2020) 103566.

[29] C.M. Domínguez, P. Ocón, A. Quintanilla, J.A. Casas, J.J. Rodriguez, Highly efficient application of activated carbon as catalyst for wet peroxide oxidation, Applied Catalysis B: Environmental 140–141 (2013) 663-670.

[30] A. Quintanilla, J.L. Díaz de Tuesta, C. Figueruelo, M. Munoz, J.A. Casas, Condensation by-products in wet peroxide oxidation: fouling or catalytic promotion? Part I. Evidences of an autocatalytic process, Catalysts (2019).

[31] A.L. Garcia-Costa, J.A. Zazo, J.J. Rodriguez, J.A. Casas, Microwave-assisted catalytic wet peroxide oxidation. Comparison of Fe catalysts supported on activated carbon and g-alumina, Appl. Catal. B 218 (2017) 637-642.

[32] C. Muranaka, C. Julcour, A. Wilhelm, H. Delmas, C.A.O. Nascimento, Regeneration of activated carbon by (photo)-Fenton oxidation, Ind. Eng. Chem. Res. 49 (2010) 989-995.

[33] Q. Chen, H. Liu, Z. Yang, D. Tan, Regeneration performance of spent granular activated carbon for tertiary treatment of dyeing wastewater by Fenton reagent and hydrogen peroxide, J. Mater. Cycles Waste Manage. 19 (2017) 256-264.

[34] S.G. Huling, E. Kan, C. Wingo, Fenton-driven regeneration of MTBE-spent granular activated carbon—Effects of particle size and iron amendment procedures, Appl. Catal. B 89 (2009) 651-658.

[35] E. Kan, S.G. Huling, Effects of Temperature and Acidic Pre-Treatment on Fenton-Driven Oxidation of MTBE-Spent Granular Activated Carbon, Environ. Sci. Technol. 43 (2009) 1493-1499.

[36] B. Calderon, F. Smith, I. Aracil, A. Fullana, Green synthesis of thin shell carbon-encapsulated iron nanoparticles via hydrothermal carbonization, ACS Sustainable Chem. Eng. 6 (2018) 7995-8002.

[37] H.T. Gomes, S.M. Miranda, M.J. Sampaio, A.M.T. Silva, J.L. Faria, Activated carbons treated with sulphuric acid: Catalysts for catalytic wet peroxide oxidation, Catal. Today 151 (2010) 153-158.

[38] C.H. Giles, T.H. MacEwan, S.N. Nakhwa, D. Smith, 786. Studies in adsorption. Part XI. A system of classification of solution adsorption isotherms, and its use in diagnosis of adsorption mechanisms and in measurement of specific surface areas of solids, J. Chem. Soc. (1960) 3973-3993.

[39] S. Álvarez-Torrellas, M. Munoz, J. Gläsel, Z.M. de Pedro, C.M. Domínguez, J. García, B.J.M. Etzold, J.A. Casas, Highly efficient removal of pharmaceuticals from water by well-defined carbide-derived carbons, Chem. E. J. 347 (2018) 595-606.

[40] E. Çaliskan, S. Göktürk, Adsorption characteristics of sulfamethoxazole and metronidazole on activated carbon, Sep. Sci. Technol. 45 (2010) 244-255.

[41] X. Hu, Z. Cheng, Removal of diclofenac from aqueous solution with multi-walled carbon nanotubes modified by nitric acid, Chin. J. Chem. Eng. 23 (2015) 1551-1556.

[42] S. Álvarez, R.S. Ribeiro, H.T. Gomes, J.L. Sotelo, J. García, Synthesis of carbon xerogels and their application in adsorption studies of caffeine and diclofenac as emerging contaminants, Chem. Eng. Res. Des. 95 (2015) 229-238.

[43] S. Álvarez-Torrellas, A. Rodríguez, G. Ovejero, J. García, Comparative adsorption performance of ibuprofen and tetracycline from aqueous solution by carbonaceous materials, Chem. Eng. J. 283 (2016) 936-947.

[44] M. Munoz, F.J. Mora, Z.M. de Pedro, S. Alvarez-Torrellas, J.A. Casas, J.J. Rodriguez, Application of CWPO to the treatment of pharmaceutical emerging pollutants in different water matrices with a ferromagnetic catalyst, J. Hazard. Mater. 331 (2017) 45-54.

[45] E. Serrano, M. Munoz, Z.M. de Pedro, J.A. Casas, Efficient removal of the pharmaceutical pollutants included in the EU Watch List (Decision 2015/495) by modified magnetite/H_2O_2, Chem. Eng. J. 376 (2018) 120265.